Res Chem Intermed (2011) 37:747–757
DOI 10.1007/s11164-011-0321-z

Nickel-catalyzed synthesis of nanoporous organic frameworks and their potential use in gas storage applications

Refaie M. Kassab · Karl T. Jackson · Oussama M. El-Kadri · Hani M. El-Kaderi

Received: 1 February 2011 / Accepted: 29 April 2011 / Published online: 18 May 2011

Abstract The synthesis of highly nanoporous organic frameworks (NPOFs) has been established using nickel(0)-catalyzed Yamamoto coupling reactions, which has afforded highly porous polymers featuring remarkable chemical and thermal stability. Treatment of 1,3,5-tris(4-bromophenyl)benzene, 1,2,4,5-tetrakis(4-bromophenyl)benzene, or 1,3,5,7-tetrakis(4-iodophenyl)adamantane with $Ni(cod)_2$ in DMF at 80°C for 48 h afforded the nanoporous organic frameworks, NPOF-1, NPOF-2, and NPOF-3, respectively, as white powders in quantitative yields. All NPOFs are insoluble in common organic solvents such as dimethylformamide, tetrahydrofuran, toluene, dichloromethane, and methanol. The chemical composition and structural aspects of NPOFs were investigated by spectral and analytical methods while porosity was examined by nitrogen porosity measurements. In spite of their amorphous nature, NPOFs exhibit permanent porosity and high Langmuir surface areas (NPOF-1: 2,635 $m^2\ g^{-1}$; NPOF-2: 4,227 $m^2\ g^{-1}$; NPOF-3: 2,423 $m^2\ g^{-1}$), which make them attractive for subsequent use in gas storage and separation applications, among others. The performance of NPOFs in hydrogen storage was evaluated at 1 bar and 77 K and revealed that these highly porous architectures can store up to 1.45 wt% of hydrogen.

R. M. Kassab · K. T. Jackson · O. M. El-Kadri · H. M. El-Kaderi (✉)
Department of Chemistry, Virginia Commonwealth University, Richmond, VA 23284-2006, USA
e-mail: helkaderi@vcu.edu

R. M. Kassab
Chemistry Department, Faculty of Science, Cairo University, Giza, Egypt

Present Address:
O. M. El-Kadri
Department of Biology and Chemistry, American University of Sharjah, 26666, Sharjah, United Arab Emirates

Keywords Nanoporous · Organic polymers · Hydrogen storage · High surface area · Yamamoto coupling

Introduction

The design and synthesis of highly porous organic polymers with predefined porosity has attracted considerable attention due to their potential in applications that entail gas storage and separation, catalysis, and conductivity [1–4]. Among this class of materials are covalent-organic frameworks (COFs), which can be tailored to possess exceptional porosities, very low densities, and pore metrics that span the micro- and meso-porous ranges [5–13]. The crystalline nature of COFs stem from the dynamic nature of covalent bonds involved in their construction. Unfortunately, the dynamic nature of B–O bonds in COFs renders them prone to hydrolysis, which leads to framework decomposition and loss of porosity. In the absence of reversible bond formation, covalently linked polymers lack long-range ordering and tend to be amorphous. Nevertheless, such polymers can be designed to possess well-defined cavities through the use of building blocks that dictate the spatial growth of the polymer. Interestingly, high surface areas are typically imparted to these porous architectures without the use of templating processes. Recent efforts in this field have been directed towards the synthesis of more thermally and chemically robust materials in order to enhance material durability [14–41]. For example, Ben et al. [27] used the nickel(0)-catalyzed Yamamoto coupling reaction to link tetrahedral monomers (tetraphenylmethane) by C–C bond into a highly porous aromatic framework, PAF-1. PAF-1 has high specific surface area (Langmuir surface area: 7,100 $m^2\ g^{-1}$), remarkable thermal and chemical stability, and remains the most porous purely organic material reported to date. Moreover, the oxidative Eglinton coupling of terminal alkynes has been utilized for the construction of alkyne-linked frameworks such as porous polymer networks (PPNs) reported by Zhou and coworkers [38], which also exhibited high Langmuir surface areas (827–2,790 $m^2\ g^{-1}$). The same report also described the synthesis of PPN-3 (5,323 $m^2\ g^{-1}$) by linking tetraphenyladamantane using the same method reported by Ben et al. Cooper et al. have synthesized porous poly(aryleneethynylene) networks using palladium-catalyzed Sonogashira–Hagihara cross-coupling [18–31]. These conjugated microporous polymers (CMPs) are amorphous and have Brunauer–Emmett–Teller (BET) surface areas of up to 834 $m^2\ g^{-1}$. It has been reported that the use of unfused benzene rings in the pore walls of porous architectures is essential for obtaining exceptionally high porosity [42]. Introducing high porosity into materials has a direct impact on several applications including hydrogen storage by physisorption in particular [43]. Hydrogen storage remains one of the major hurdles facing the widespread use and commercialization of this highly flammable fuel [44–46]. There have been intensive research efforts in this area to meet targets set by the US Department of Energy for on-board hydrogen storage for 2015 (volumetric 40 g l^{-1}; gravimetric 5.5 wt%) [47].

With these considerations in mind, we report herein on the synthesis and characterization of highly porous organic polymers using nickel-catalyzed

Yamamoto coupling reactions. The use of various building blocks with a variable number of unfused benzene rings leads to enhanced porosity. The resultant polymers are chemically and thermally robust and most importantly permanently porous with very high surface areas, which makes them an ideal candidate for hydrogen storage applications.

Experimental

Materials and methods

All starting materials, unless noted otherwise, were obtained from Thermo Fisher Scientific Inc. and used without further purification. Anhydrous DMF (99.98%) was purchased from Acros Chemicals. 1,5-cyclooctadiene (COD) was distilled from calcium hydride, and toluene was distilled from sodium. 1,3,5,7-tetrakis (4-iodophenyl)adamantane, 1,3,5-tris(4-bromophenyl)benzene, and 1,2,4,5-tetrakis (4-bromophenyl)benzene were prepared according to literature methods [46–51]. All reactions were performed under a nitrogen atmosphere using glovebox or Schlenk line techniques. Elemental analyses were performed by Midwest Microlab, Indianapolis, IN. (*Lower carbon contents are due to unreacted halide at the surface of the polymers or unreacted starting material inside pores*) [38]. FT-IR spectra were collected using KBr pellets in transmission mode using a Nicolet Nexus 670 spectrometer. All spectra were measured with 32 scans at a resolution of 4 cm^{-1} using a blank KBr disk as background, followed by baseline correction. Thermogravimetric analysis (TGA) was carried out using a Q5000IR analyzer (TA Instruments). The samples were heated at the rate of 5 °C/min under a nitrogen atmosphere up to 700°C. Powder X-ray diffraction data were collected on a Panalytical X'pert pro multipurpose diffractometer (MPD). Samples were mounted on a zero-background sample holder and measured using Cu Kα radiation with a 2θ range of 5–30. Scanning electron microscopy (SEM) images were taken on a Hitachi SU-70 scanning electron microscope. The samples were mounted onto aluminum holders, and then coated with platinum at 1×10^{-4} mbar of pressure in a nitrogen atmosphere for 120 s before imaging. Solid-state nuclear magnetic resonance (NMR) spectra were recorded at ambient temperature on a 363-MHz NMR system. ^{13}C CP-MAS spectra were obtained with a 1-ms contact time and a 3-s recycle delay.

Gas sorption analysis

Low-pressure N_2 and H_2 adsorption measurements (0–1 bar and 77 K) were performed on an Autosorb-1 C (Quantachrome) volumetric analyzer. All samples were degassed at 200°C/10^{-5} Torr for 12 h before analysis. Ultra-high-purity grade N_2 and H_2 (99.999% purity) were used throughout the adsorption experiments. Surface areas were calculated in the relative pressure (P/P_o) range from 0.05 to 0.3. Pore size distributions (PSDs) and pore volumes were derived from N_2 adsorption branches using the nonlocal density functional theory (NLDFT) cylindrical pore model.

Synthesis of nanoporous organic frameworks-1 (NPOF-1)

To a 250-mL Schlenk flask equipped with a stir bar was added COD (520 mg, 4.8 mmol), $Ni(cod)_2$ (1.32 g, 4.80 mmol), 2,2′-bipyridyl (750 mg, 4.80 mmol), and DMF (60 ml). The mixture was heated at 80°C for 1 h to afford a dark purple solution. To the resultant solution was added 1,3,5-Tris(4-bromophenyl)benzene (500 mg, 0.92 mmol) in DMF (20 ml) and the resultant suspension was kept stirring for an additional 24 h at 80°C. The mixture was cooled to room temperature and the dark residue was filtered off over a medium glass frit. Concentrated HCl (12 M, 20 ml) was added dropwise to the residue. Afterwards, the residue was washed with acetone (5 × 10 ml), $CHCl_3$ (5 × 10 ml), THF (5 × 10 ml) and H_2O (5 × 10 ml), respectively, and dried under reduced pressure to afford NPOF-1 as an off-white powder (460 mg, 99% based on 1,3,5-Tris(4-bromophenyl)benzene); Anal. Calcd. for C_8H_5: C, 95.02; H, 4.98. Found: C, 89.95; H, 5.53. FT-IR (ν, cm^{-1}) 3,434 (s, br), 3,034 (w), 2,925 (w), 1606 (m), 1,496 (m), 1,112 (m), 992 (s), 811 (s); H 5.04. ^{13}C CP-MAS (400 MHz) $\delta = 140.3$, 126.6.

Synthesis of nanoporous organic frameworks-2 (NPOF-2)

In a fashion similar to the preparation of NPOF-1, COD, (484 mg, 4.5 mmol), $Ni(cod)_2$ (1.24 g, 4.5 mmol), 2,2-bipyridyl (703 mg, 4.5 mmol), and DMF (60 ml) were combined. The mixture was heated at 80°C for 1 h. To the resulting purple solution was added a DMF (20 ml) solution of 1,2,4,5-Tetrakis(4-bromophenyl)benzene (0.86 mmol, 600 mg). Post-synthesis treatment and isolation afforded NPOF-2 as an off-white powder (510 mg, 95% yield). Anal. Calcd. for C_5H_3: C, 95.21; H, 4.79. Found: C, 88.95; H, 5.20. FT-IR (ν, cm^{-1}) 3,433 (s, br), 3,034 (m), 1,606 (m), 1,491 (s), 1,201 (w), 992 (s), 811 (s), 744 (w), 702 (w); ^{13}C CP-MAS (400 MHz) $\delta = 146.0$, 139.1, 130.7, 125.1.

Synthesis of nanoporous organic frameworks-3 (NPOF-3)

In a fashion similar to the preparation of NPOF-1, COD, (310 mg, 2.73 mmol), $Ni(cod)_2$ (750 mg, 2.73 mmol), 2,2-bipyridyl (430 mg, 2.73 mmol), and DMF (60 ml) were combined. The mixture was heated at 80°C for 1 h. To the resulting purple solution was added a DMF (20 ml) solution of 1,3,5,7-Tetrakis(4-iodophenyl) adamantane (0.53 mmol, 500 mg). Post-synthesis treatment and isolation afforded NPOF-3 as an off-white powder (217 mg, 94%). Anal. Calcd. for $C_{34}H_{27}$: C, 93.75; H, 6.25. Found: C, 87.69; H, 6.35. FT-IR (ν, cm^{-1}) 3,439 (s, br), 3,034 (s), 2,930 (s), 2,847 (s), 1,606 (m), 1,507 (s), 1,449 (m), 1,351 (s), 1,091 (s), 998 (s), 821 (s), 738 (m), 691 (m), 557 (m), 468 (m); ^{13}C CP-MAS (400 MHz) $\delta = 147.8$, 125.2, 47.7, 45.4, 38.9.

Results and discussion

The synthesis of NPOFs was established using methods described by Ben et al. and the monomeric building units were specifically chosen to increase the surface area

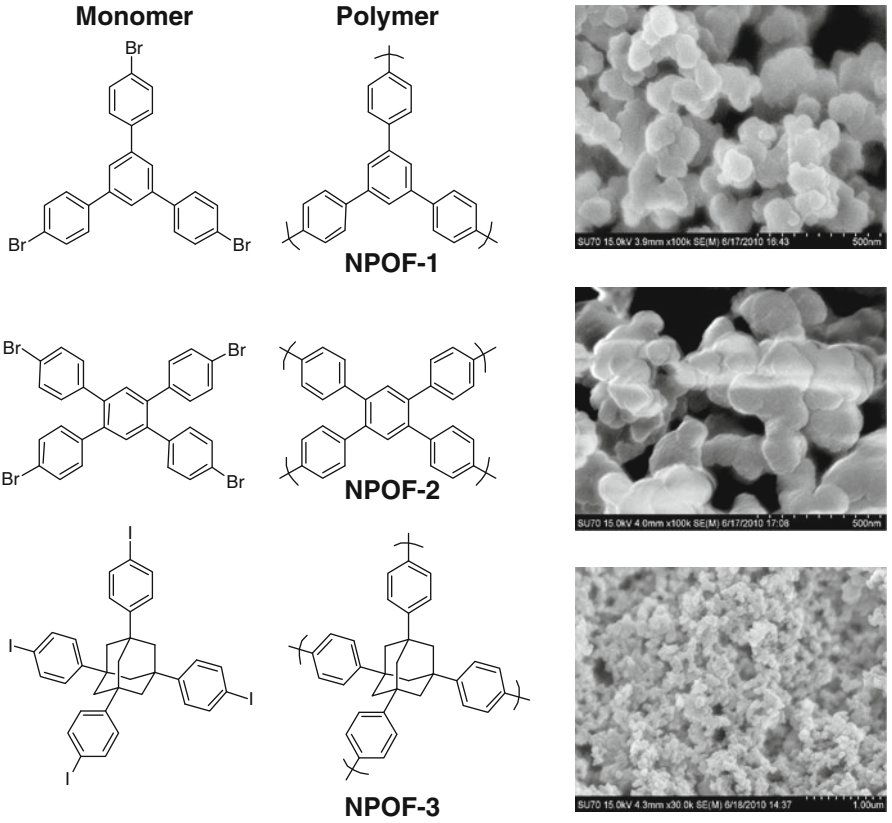

Fig. 1 2-D and 3-D monomers used for the construction of NPOF-1, NPOF-2, and NPOF-3 and their respective SEM images. All coupling reactions were performed under an inert atmosphere in DMF at 80°C using $Ni(COD)_2$

of the resultant polymers for subsequent use in adsorptive hydrogen storage studies (Fig. 1). NPOFs are insoluble in common organic solvents such as dimethylformamide, tetrahydrofuran, toluene, dichloromethane, methanol, and acetone, which facilitate their purification steps. Additionally, NPOFs exhibit a remarkable chemical stability and remain intact in 12 M HCl or 6 M NaOH solutions.

The chemical composition and structural aspects of NPOFs were investigated by spectral and analytical methods while their porous nature was examined by N_2 porosity measurements. Unlike COFs, all NPOFs were amorphous, which prevented their solid-state investigation by powder X-ray diffraction techniques. Amorphous materials are generally obtained, as in the case of organic polymers such as polymers of intrinsic microporosity (PIMs), CMPs, PPNs, etc., due to the lack of bond formation reversibility.

In spite of their lack of long-range ordering, these polymers can be highly porous and suitable for multifaceted applications. To investigate phase purity of NPOFs, we collected SEM images, which revealed that NPOF-1 and NPOF-2 exist as platelets of $\sim$200–300 nm in size. The formation of platelet morphology is most likely due

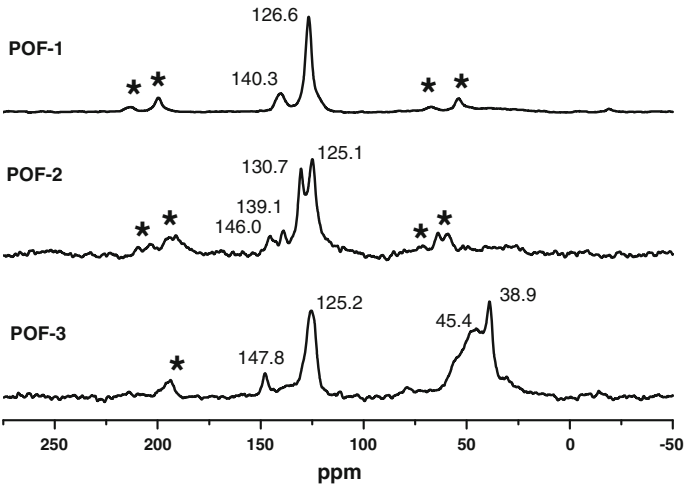

Fig. 2 ^{13}C CP-MAS NMR spectra of activated NPOFs. Signals assigned with *asterisks* denote spinning sidebands

to the 2-D nature of the NPOF-1 and NPOF-2 frameworks that are facilitated by π-staking of the conjugated phenyl rings. In contrast, the particles of NPOF-3 are more spherical as a result of the 3-D building unit (tetraphenyladamantane) employed for the construction of this framework. The chemical composition of NPOFs was first investigated by elemental analysis, which provided lower carbon contents than expected for all NPOFs. A similar observation has been reported for other materials constructed using coupling reactions that entail aryl halides as in the case of CMPs and PPNs. The lower carbon contents recorded for all NPOFs may originate from trapped starting materials inside the pores or unreacted halides at the surface of the polymers [18–31, 38]. It has been suggested that the surface of such polymers is terminated by unreacted carbon-halide bonds, however their concentrations are very low, which does not allow for their detection by NMR methods. The presence of carbon-halide in NPOFs was supported by FT-IR spectroscopy studies, which revealed vibration stretches at $\sim$750 cm^{-1} that are consistent with aryl halide functionality.

To establish the incorporation of monomeric building units into NPOF networks through the formation of C–C bonds, we collected solid-state ^{13}C CP-MAS NMR experiments on activated samples (Fig. 2). CP-MAS NMR techniques have been widely used for the characterization of porous organic materials, especially amorphous polymers, to help illustrate their solid-state structure and connectivity between building units. The activation process of NPOFs involved treatment with 12 M HCl followed by washing with organic solvents and water to remove residual nickel and soluble oligomers or starting materials. After several washing steps, NPOFs were subjected to heating under reduced pressure (200°C/10^{-5} Torr) for 12 h. In all spectra, the ^{13}C signals at $\sim\delta = 122$ ppm (C–Br) or 94 ppm (C–I) that correspond to the carbon-halide in the starting monomers were absent and under NMR detection levels. In the ^{13}C CP MAS spectrum of NPOF-1, the signals at

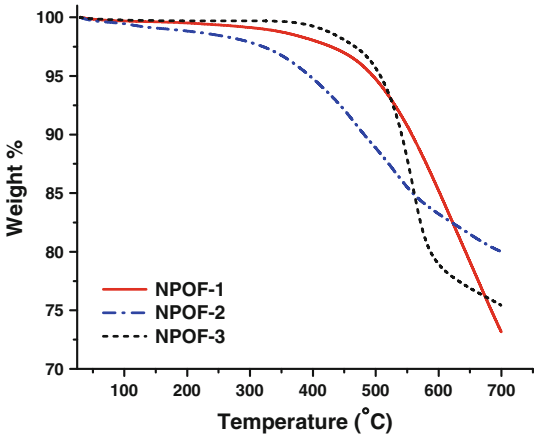

Fig. 3 TGA of activated NPOFs revealing their remarkable thermal stability up to ~450°C

$\delta = 140.2$ and 126.6 ppm correspond to the new C–C bond formed upon aryl–aryl coupling and the *ortho*-CH carbon, respectively, while the signal for C–Br that usually appears at $\delta = 122.3$ ppm is absent. In the spectrum of NPOF-2, the signals at $\delta = 146.0$ and 139.1 ppm correspond to the new C–C bond formed while signals at 130.7 and 125.1 ppm correspond to the *ortho*-CH carbons. Also, the C–Br signal at $\delta = 121.4$ ppm is absent. For NPOF-3, the signal at $\delta = 147.8$ and 125.2 ppm correspond to the new C–C bond formed and the *ortho*-CH carbon, respectively. Also, the C–I signal at $\delta = 91.7$ ppm is absent. The covalent nature of NPOFs was also manifested in their high thermal stability during TGA studies (Fig. 3). TGA traces collected from studies conducted on activated samples revealed that NPOF-1 and NPOF-3 remain stable up to ~450°C, whereas NPOF-2 starts to decompose about 350°C. These decomposition temperatures are typical for covalent polymers that show higher thermal stability than most of their MOF counterparts. This feature makes NPOFs very attractive for use in industrial applications where thermal and chemical stability is generally needed.

Of particular interest to us is the ability to tailor the porosity in NPOFs and to investigate its impact on the physisorption of dihydrogen, which has been under intensive investigation, as it represents a clean and renewable energy source. The porosity of NPOFs was established using N_2 sorption–desorption experiments on the activated materials. NPOF samples were degassed at 200°C and 10^{-5} Torr for 12 h prior to nitrogen sorption analysis. The nitrogen uptakes depicted in Fig. 4 indicate that NPOFs have permanent porosity evidenced by the fully reversible uptake-release of nitrogen for all materials. The steep rise in the nitrogen uptake at $P/P_o = 0$–0.1 and the type I isotherms indicate microporosity. There is notable hysteresis for all samples and a gradual increase in nitrogen uptake until saturation pressure ($P/P_o = 1$), which may indicate that NPOFs have a flexible "soft" nature [36]. Surface area measurements were conducted using the adsorption branch from the N_2 isotherms at $P/P_o = 0.05$–0.30 and are listed along with other textural properties in Table 1. NPOFs exhibit considerably high Langmuir surface area values: 2,635 $m^2\ g^{-1}$ (NPOF-1); 4,227 $m^2\ g^{-1}$ (NPOF-2); and 2,423 $m^2\ g^{-1}$ (NPOF-3). PSD was calculated using NLDFT using the uptake branch of the

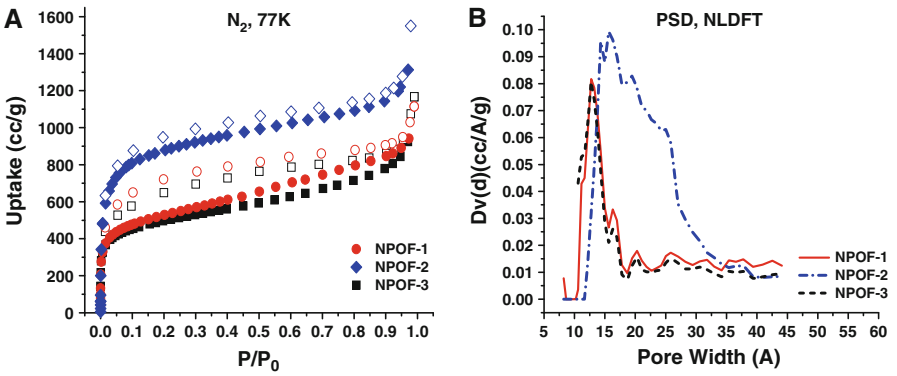

Fig. 4 Nitrogen uptake isotherms (**a**); adsorption (*filled*) and desorption (*empty*) at 77 K and 0–1 bar. PSD calculated using NLDFT (**b**)

Table 1 Porous properties and hydrogen uptake of NPOFs

Polymer	SA_{Lang} (m^2 g^{-1})[a]	SA_{BET} (m^2 g^{-1})[b]	P_{vol} (cm^3/g)[c]	PSD (nm)[d]	H_2 (wt%)
NPOF-1	2,635	1,907	1.5722	1.27	1.28
NPOF-2	4,227	3,127	2.4418	1.56	1.45
NPOF-3	2,423	1,794	1.1925	1.27	0.82

[a] Calculated by the Langmuir method

[b] Calculated by the BET method

[c] Calculated from nitrogen adsorption branch at $P/P_o = 0.9$

[d] Calculated from NLDFT

nitrogen isotherm [52]. Both NPOF-1 and NPOF-3 show a narrow PSD of about 1.27 nm while NPOF-2 exhibits a boarder PSD in the range of 1.56–2.50 nm and therefore has both micro- and mesopores. It was surprising to us to see that NPOF-3 has a lower surface area than its related PPN-3 (5,323 m^2 g^{-1}) that was synthesized using 1,3,5,7-Tetrakis(4-bromophenyl)adamantane under similar reaction conditions. The lower surface area observed for NPOF-3 may result form a faster coupling rate associated with the iodo-building block, 1,3,5,7-Tetrakis(4-iodophenyl)adamantine, which could hamper organized pore formation and the overall porosity of NPOF-3. The experimental surface areas (SA_{BET}) for NPOFs were compared against those of purely organic porous materials such as CMPs, PPNs, COFs, and PIMs. The surface area of NPOFs, especially that of NPOF-2, exceeds that of most of PIMs (430–1,760 m^2 g^{-1}), or CMPs (522–1,631 m^2 g^{-1}) and are similar to those of highly porous 3-D COFs (e.g., COF-103, ~4,210 m^2 g^{-1}), PAF-1 (5,600 g^{-1}) and PPNs (1,249–2,840 m^2 g^{-1}).

Hydrogen storage remains one of the major hurdles facing the widespread use and commercialization of this highly flammable fuel. It is now well recognized that physisorption of H_2 is a function of surface area in porous materials such as organic polymers, MOFs, COFs, etc. Given the high surface areas of NPOFs, we investigated their low-pressure hydrogen storage performance at 77 K and

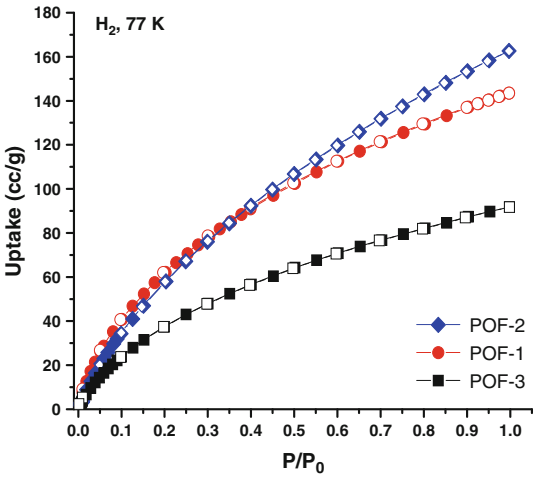

Fig. 5 Hydrogen uptake isotherms for NPOFs; adsorption (*filled*) and desorption (*empty*) at 77 K and 0–1 bar

0–1 bar (Fig. 5). The H_2 uptakes listed in Table 1 were higher for NPOFs of higher surface area as expected, and the PSD seems to have a modest impact on the final uptake at the above-mentioned conditions. Previous studies have documented the impact of pore size on hydrogen storage, which can be enhanced by pores having dimensions close to the kinetic diameter of the H_2 molecule. The storage enhancement is a result of increased interaction between the H_2 and the pore walls. Even though NPOF-1 and NPOF-3 have relatively smaller pores than NPOF-2, the storage capability of the latter exceeds the other NPOFs due to its higher surface area. We have also compared hydrogen storage by NPOFs to other related organic and inorganic porous architectures. For example, under similar conditions, the related COFs and CTFs store 0.9–1.2 and 1.55 wt% of H_2, respectively [11, 14]. Other purely organic polymers such as hypercrosslinked polymer networks synthesized by the self-condensation of bischloromethyl monomers (0.89–1.69 wt%), nitrogen-linked nanoporous networks of aromatic rings (0.01–0.85 wt%) [53], and PIMs, which recently have been reported to be among the best organic polymers for hydrogen uptake (0.74–1.83 wt%), show comparable uptakes [54]. Moreover, the H_2 uptakes of NPOFs are in line with those recently reported for PAF-1 (1.5 wt%) or PPNs (1.37–1.58 wt%). In contrast, activated carbon such as PICACTIF-SC, AX-21, and zeolite-templated show higher uptake (1.90, 2.40, and 2.60 wt%, respectively) [55, 56]; however, we anticipate NPOFs to exhibit higher hydrogen uptake under high-pressure and cryogenic conditions.

Conclusions

In conclusion, a series of highly porous organic polymers of permanent porosity and high thermal and chemical stability has been prepared using nickel-catalyzed Yamamoto coupling reactions of 2-D and 3-D aryl halide building blocks. The surface areas and pore sizes in these polymers are directly impacted by the

dimensionality and metrics of the building blocks. We anticipate these polymers to undergo post-synthesis chemical modification that would install several functional groups into the pore wall which could enhance gas uptake and selectivity, ion-capture, and separation applications. The accessible high surface area in NPOFs makes them attractive for high-pressure gas uptake studies, which are currently being addressed in our laboratory.

Acknowledgments We are grateful to the US Department of Energy (DE-SC0002576) for generous support of this project. H.M. El-Kaderi acknowledges support of the Donors of the American Chemical Society Petroleum Research Fund ACS-PRF (48672-G5).

References

1. N.B. McKeown, P.M. Budd, Macromolecules **43**, 5163 (2010)
2. N.B. McKeown, P.M. Budd, Chem. Soc. Rev. **35**, 675 (2006)
3. A. Thomas, P. Kuhn, J. Weber, M.-M. Titirici, M. Antonietti, Macromol. Rapid Commun. **30**, 221 (2009)
4. K.E.J. Maly, Mater. Chem. **19**, 1781 (2009)
5. A.P. Côté, A.I. Benin, N.W. Ockwig, M. O'Keeffe, A.J. Matzger, O.M. Yaghi, Science **310**, 1166 (2005)
6. W.R. Tilford, W.R. Gemmil, H.C. zur Loye, J.J. Lavigne, Chem. Mater. **18**, 5296 (2006)
7. H.M. El-Kaderi, J.R. Hunt, J.L. Mendoza-Cortés, A.P. Côté, R.E. Taylor, M. O'Keeffe, O.M. Yaghi, Science **316**, 268 (2007)
8. A.P. Côté, H.M. El-Kaderi, H. Furukawa, J.R. Hunt, O.M. Yaghi, J. Am. Chem. Soc. **129**, 12914 (2007)
9. S. Wan, J. Guo, J. Kim, H. Ihee, D. Jiang, Angew. Chem. Int. Ed. **47**, 8826 (2008)
10. S. Wan, J. Guo, J. Kim, H. Ihee, D. Jiang, Angew. Chem. Int. Ed. **48**, 5439 (2009)
11. H. Furukawa, O.M. Yaghi, J. Am. Chem. Soc. **25**, 8876 (2009)
12. F.J. Uribe-Romo, J.R. Hunt, H. Furukawa, C. Klock, M. O'Keeffe, O.M. Yaghi, J. Am. Chem. Soc. **131**, 4570 (2009)
13. J.R. Hunt, C.J. Doonan, J.D. LeVangie, A.P. Côté, O.M. Yaghi, J. Am. Chem. Soc. **130**, 11872 (2008)
14. P. Kuhn, M. Antonietti, A. Thomas, Angew. Chem. Int. Ed. **47**, 3450 (2008)
15. P. Kuhn, A. Thomas, M. Antonietti, Macromolecules **42**, 319 (2009)
16. M.J. Bojdys, J. Jeromenok, A. Thomas, M. Antonietti, Adv. Mater. **22**, 2202 (2010)
17. M.J. Bojdys, S.A. Wohlgemuth, A. Thomas, M. Antonietti, Macromolecules **43**, 6639 (2010)
18. J.X. Jiang, F. Su, C.D. Wood, N.L. Campbell, H. Niu, C. Dickinson, A.Y. Ganin, M.J. Rosseinsky, Y.Z. Khimyak, A.I. Cooper, A. Trewin, Angew. Chem. Int. Ed. **46**, 8584 (2007)
19. J.X. Jiang, F. Su, C.D. Wood, A. Trewin, H. Niu, J.T.A. Jones, Y.Z. Khimyak, A.I. Cooper, J. Am. Chem. Soc. **130**, 7710 (2008)
20. R. Dawson, F. Su, H. Niu, C.D. Wood, J.T.A. Jones, Y.Z. Khimyak, A.I. Cooper, Macromolecules **41**, 1591 (2008)
21. J. Weber, A. Thomas, J. Am. Chem. Soc. **130**, 6334 (2008)
22. J.X. Jiang, F. Su, H. Niu, C.D. Wood, N.L. Campbell, Y.Z. Khimyak, A.I. Cooper, Chem. Commun. 486 (2008)
23. R. Dawson, A. Laybourn, R. Clowes, Y.Z. Khimyak, D.J. Adams, A.I. Cooper, Macromolecules **42**, 8809 (2009)
24. A.I. Cooper, Adv. Mater. **21**, 1291 (2009)
25. S. Yuan, S. Kirklin, B. Dorney, D.J. Liu, L. Yu, Macromolecules **42**, 1554 (2009)
26. J. Schmidt, M. Werner, A. Thomas, Macromolecules **42**, 4426 (2009)
27. T. Ben, H. Ren, S. Ma, D. Cao, J. Lan, X. Jing, W. Wang, J. Xu, F. Deng, J.M. Simmons, S. Qiu, G. Zhu, Angew. Chem. Int. Ed. **48**, 9457 (2009)
28. L. Chen, Y. Honsho, S. Seki, D. Jiang, J. Am. Chem. Soc. **132**, 6742 (2010)
29. J. Xia, S. Yuan, Z. Wang, S. Kirklin, B. Dorney, D.J. Liu, L. Yu, Macromolecules **43**, 3325 (2010)

30. R. Dawson, A. Laybourn, Y.Z. Khimyak, D.J. Adams, A.I. Cooper, Macromolecules **43**, 8524 (2010)
31. R.S. Sprick, A. Thomas, U. Scherf, Polym. Chem. **1**, 283 (2010)
32. P.M. Budd, B.S. Ghanem, S. Makhseed, N.B. McKeown, K.J. Msayib, C.E. Tattershall, Chem. Commun. **2**, 230 (2004)
33. N.B. McKeown, B. Gahnem, K.J. Msayib, P.M. Budd, C.E. Tattershall, K. Mahmood, S. Tan, D. Book, H.W. Langmi, A. Walton, Angew. Chem. **118**, 1836 (2006)
34. N.B. McKeown, B. Gahnem, K.J. Msayib, P.M. Budd, C.E. Tattershall, K. Mahmood, S. Tan, D. Book, H.W. Langmi, A. Walton, Angew. Chem. Int. Ed. **45**, 1804 (2006)
35. P. Kuhn, M. Antonietti, A. Thomas, Angew. Chem. **120**, 3499 (2008)
36. J. Weber, M. Antonietti, A. Thomas, Macromolecules **41**, 2880 (2008)
37. M.G. Schwab, B. Fassbender, H.W. Spiess, A. Thomas, X.L. Feng, K. Mullen, J. Am. Chem. Soc. **131**, 7216 (2009)
38. W. Lu, D. Yuan, D. Zhao, C.I. Schilling, O. Plietzsch, T. Muller, S. Brase, J. Guenther, J. Blumel, R. Krishna, Z. Li, H. Zhou, Chem. Mater. **22**, 5964 (2010)
39. O.K. Farha, A.M. Spokoyny, B.G. Hauser, Y. Bae, S.E. Brown, R.Q. Snurr, C.A. Mirkin, J.T. Hupp, Chem. Mater. **21**, 3033 (2009)
40. O.K. Farha, A.M. Spokoyny, B.G. Hauser, Y. Bae, R.Q. Snurr, C.A. Mirkin, J.T. Hupp, Chem. Commun. **46**, 1056 (2010)
41. A. Trewin, A.I. Cooper, Angew. Chem. Int. Ed. **49**, 1533 (2010)
42. H. Furukawa, N. Ko, Y.B. Go, N. Aratani, S.B. Choi, E. Choi, A.O. Yazaydin, R.Q. Snurr, M. O'Keeffe, J. Kim, O.M. Yaghi, Science **329**, 424 (2010)
43. J. Germain, F. Svec, J.M.J. Fréchet, Small **5**, 1098 (2009)
44. L. Schlapbach, A. Zuttel, Nature **414**, 353 (2001)
45. D.J. Collins, H.C. Zhou, J. Mater. Chem. **17**, 3154 (2007)
46. A. Klerke, C.H. Christensen, J.K. Nørskov, T. Vegge, J. Mater. Chem. **18**, 2304 (2008)
47. DOE Targets for On-Board Hydrogen Storage Systems for Light-Duty Vehicles, https://www1.eere.energy.gov/hydrogenandfuelcells/storage/pdfs/targets_onboard_hydro_storage_explanation.pdf
48. X.Y. Cao, X.H. Liu, X.H. Zhou, Y. Zhang, Y. Jiang, Y. Cao, Y.X. Cui, J. Pei, J. Org. Chem. **69**, 6050 (2004)
49. Z.H. Li, M.S. Wong, Y. Tao, Tetrahedron **61**, 5277 (2005)
50. R. Rathore, C.L. Burns, Org. Synth. **82**, 30 (2005)
51. V.R. Reichert, L.J. Mathias, Macromolecules **27**, 7015 (1994)
52. R.I. Ravikovitch, A. Vishnyakov, R. Russo, A.V. Neimark, Langmuir **16**, 2311 (2000)
53. J. Germain, F. Svec, J.M.J. Fréchet, Chem. Mater. **20**, 7069 (2008)
54. B.S. Ghanem, M. Hashem, K.D.M. Harris, K.J. Msayib, M.C. Xu, P.M. Budd, N. Chaukura, D. Book, S. Tedds, A. Walton, N.B. McKeown, Macromolecules **43**, 5287 (2010)
55. N. Texier-Mandoki, J. Dentzer, T. Piquero, S. Saadallah, P. David, C. Vix-Guterl, Carbon **42**, 2744 (2004)
56. Z.X. Yang, Y.D. Xia, R. Mokaya, J. Am. Chem. Soc. **129**, 1673 (2007)